Universal Model and Control Framework for Bearingless Motors with Combined Windings

Takahiro NOGUCHI*, Mohamadhasan MOKHTARABADI*, Kamisetti N V PRASAD*,
Wolfgang GRUBER** and Eric L. SEVERSON*
* Department of Mechanical Engineering, University of Minnesota
111 Church St SE, Minneapolis, Minnesota, USA
E-mail: tnoguchi@umn.edu
** Institute of Electric Drives and Power Electronics, Johannes Kepler University Linz
Altenberger Str. 69, 4040 Linz, Austria

Abstract
This paper presents a model and control framework for bearingless motors that is generalized for all types of combined winding configurations with six phases. The aim of the paper is to facilitate the rapid implementation of MATLAB Simulink models of the electric behavior (voltage/current) and mechanical behavior (force/torque) for any bearingless motor with a combined winding. Bearingless motor developers will find this to be a useful guide for creating control simulations and understanding how changes in the number of motor/suspension poles and winding type impact their control architecture. The paper shows how the provided universal model/controller can serve as the starting point and baseline for establishing a control simulation environment that is later refined to capture the architecture-specific aspects of a practical bearingless motor control system.

Keywords : Bearingless motor, Combined winding, DPNV winding, Space vector, Simulink, Winding functions

1. Introduction

Bearingless motor development has historically been relegated to highly targeted, isolated applications with extreme needs for magnetic levitation. This includes implantable blood pumps, hygienic mixing devices, and flywheel energy storage. The wide variety of applications of differing needs has led to a fragmented approach to developing this technology: researchers investigate a unique machine topology, with a unique model and control requirements, as if it is an isolated invention. More recently, efforts have been underway to develop bearingless motors for industrial scale applications, which has resulted in publications generalizing the theory and advancements behind bearingless motors, i.e. Khamitov et al. (2023); Khamitov and Severson (2023); Gruber and Silber (2018); Silber et al. (2005). This paper will continue the trend of unifying the modeling and control approach of bearingless motors.

The primary contribution of this paper is to provide this generalized model for radial flux non-salient bearingless motors with six-phases using any combined winding configuration. The windings considered in this paper include multiphase (MP), multiphase with a dual neutral point (MP2), parallel and bridge dual-purpose no-voltage (DPNV), and mid-point current injection (MCI) windings. The paper reviews literature on these configurations and highlights the following recent advancements: 1) that all combined windings can be realized with the same stator winding pattern, but with different drive connections and control architectures; and 2) from this universal winding pattern, generalized winding functions can be expressed for each phase of the combined winding. The paper uses these generalized winding functions to create a general inductance matrix and force/torque expressions and shows how these can be combined to model the complete machine. This facilitates the development of a MATLAB Simulink model generalized to all winding types that can be configured at runtime via a script that specifies the number of pole-pairs and winding type.

The proposed framework allows bearingless motor engineers to simulate and develop control strategies for a wide range of bearingless motor configurations using a single and flexible Simulink template. The paper includes a case study to demonstrate the generalized modeling approach and provides a Simulink template that readers can download via an open source GitHub repository: `https://github.com/severson-group/bm-modeling`.

2. Multiphase combined winding bearingless motor model

Khamitov and Severson (2023) showed that MP combined windings are the most general form of combined winding and that all other combined winding types can be understood as special cases of the MP winding. For this reason, the paper first reviews and formulates the complete bearingless motor model for MP windings in this section. Later, Section 3 uses the results of this section to propose the paper's universal combined winding bearingless motor model.

This section derives force/torque and electrical (voltage, current, inductance) expressions. The derivation starts from fundamentals by using well-known winding function theory to make airgap field calculations and the Maxwell stress tensor to derive force and torque.

2.1. Airgap field calculations

Khamitov et al. (2023); Khamitov and Severson (2023) have recently shown that the idealized phase winding functions for all types of combined winding bearingless motors must be as follows:

$$N_k(\alpha) = \hat{N}_p \cos\left(p\alpha - \alpha_{\mathrm{w0},p} - [k-1]\alpha_\mathrm{t}\right) + \hat{N}_{p_\mathrm{s}} \cos\left(p_\mathrm{s}\alpha - \alpha_{\mathrm{w0},p_\mathrm{s}} - [k-1]\alpha_\mathrm{s}\right), \tag{1}$$

where p is the number of pole-pairs of the motor, p_s is the number of pole-pairs of the suspension winding, α is an arbitrary angular location in the airgap, and k indicates the phase number. The offset angles $\alpha_{\mathrm{w0},p}$ and $\alpha_{\mathrm{w0},p_\mathrm{s}}$ are included for generality in Eq. (1), but are neglected for simplicity in this paper. It is a critical result of these articles that α_s and α_t are uniquely determined by the pole-pair combination as

$$\alpha_\mathrm{t} = \mathrm{wrap}\left(p\frac{2\pi}{m}\right), \qquad \alpha_\mathrm{s} = \mathrm{wrap}\left(p_\mathrm{s}\frac{2\pi}{m}\right), \tag{2}$$

where m denotes the number of phases and the right hand side is wrapped between $-\pi$ and π rad. This paper will consider only $m = 6$ phase machines. Each phase of the winding produces a radial and tangential field. It is well-known from winding function theory that the radial field can be calculated as $B_\mathrm{w} = \mu_0 \frac{N_k(\alpha) i_k}{\delta}$ and that a winding function harmonic n of the form $N_n(\alpha) = \hat{N}_n \cos(n\alpha - \gamma)$ will also produce a tangential field of $B_{n,\mathrm{tan}}(\alpha) = -\mu_0 \frac{n\hat{N}_n}{r} i_k \sin(n\alpha - \gamma)$ when excited with current i_k, where r is the airgap radius. This paper assumes a magnetizing airgap field of $B_\delta(\alpha) = \hat{B}_\delta \cos(p\alpha - \theta)$ in the radial direction, where $\theta = p\theta_\mathrm{mech}$ and θ_mech is defined in Fig. 1a for a permanent magnet rotor.

2.2. Force and torque model

The airgap fields derived in Section 2.1 are now used with the Maxwell stress tensor to determine the force and torque that each phase winding creates on the shaft, as follows:

$$\begin{bmatrix}\sigma_\mathrm{n}\\ \sigma_\mathrm{tan}\end{bmatrix} = \begin{bmatrix}\frac{1}{2\mu_0}(B_\mathrm{n}^2 - B_\mathrm{tan}^2)\\ \frac{1}{\mu_0}B_\mathrm{n}B_\mathrm{tan}\end{bmatrix} \quad \Rightarrow \quad F_\mathrm{x} \approx \frac{rl}{2\mu_0}\int_0^{2\pi} B_n^2 \cos\alpha \mathrm{d}\alpha,\ F_\mathrm{y} \approx \frac{rl}{2\mu_0}\int_0^{2\pi} B_n^2 \sin\alpha \mathrm{d}\alpha,\ \tau = \frac{rl}{\mu_0}\int_0^{2\pi} B_\mathrm{n}B_\mathrm{tan}\mathrm{d}\alpha. \tag{3}$$

Here, l is the axial length of the rotor and B_tan^2 is considered negligibly small. When used with the winding function Eq. (1) and field expressions from Section 2.1, each phase winding is found to produce the following form of force and torque:

$$F_{\mathrm{x},k} = \hat{f} i_k \cos(\theta - [k-1]\alpha_\mathrm{s}), \qquad F_{\mathrm{y},k} = \mp \hat{f} i_k \sin(\theta - [k-1]\alpha_\mathrm{s}), \qquad \tau = -\hat{\tau} i_k \sin(\theta - [k-1]\alpha_\mathrm{t}), \tag{4}$$

where $F_{\mathrm{y},k}$ is negative for $p_\mathrm{s} = p+1$ and positive for $p_\mathrm{s} = p-1$. While $\hat{f}$ and $\hat{\tau}$ can be calculated analytically from Eq. (3), it is common to determine these from finite element analysis or hardware measurements, e.g. Sung et al. (2025).

It is common practice to present the force/torque model in the form $[F_\mathrm{x},\ F_\mathrm{y},\ \tau]^T = \mathbf{T}_\mathrm{m}(\theta)\,\mathbf{i}_m + \mathbf{M}_\mathrm{c}(\theta)$, as described in Silber et al. (2005). The $\mathbf{M}_\mathrm{c}$ matrix captures cogging force and torque of the machine and is independent of current. The phase currents are represented as the vector $\mathbf{i}_m = [i_1, i_2, i_3, i_4, i_5, i_6]^T$. The $\mathbf{T}_\mathrm{m}$ matrix is composed of the force and torque expressions in Eq. (4) and is depicted in Fig. 1b for different pole combinations, which correspond to different α_s and α_t values as calculated by Eq. (2).

When the phase winding currents are of the form Eq. (5), see (Khamitov et al., 2023, Eq. 10), the resulting shaft force and torque are calculated as Eq. (6), where F_y is positive for $p_\mathrm{s} = p+1$ and negative for $p_\mathrm{s} = p-1$.

$$i_k = \hat{I}_\mathrm{t} \cos(\theta + \phi_\mathrm{t}' - [k-1]\alpha_\mathrm{t}) + \hat{I}_\mathrm{s} \cos(\theta + \phi_\mathrm{s}' - [k-1]\alpha_\mathrm{s}) \tag{5}$$

$$F_\mathrm{x} = k_\mathrm{f}\hat{I}_\mathrm{s}\cos\phi_\mathrm{s}',\ F_\mathrm{y} = \pm k_\mathrm{f}\hat{I}_\mathrm{s}\sin\phi_\mathrm{s}',\ \tau = k_\mathrm{t}\hat{I}_\mathrm{t}\sin\phi_\mathrm{t}', \qquad \text{where: } k_\mathrm{f} = 3\hat{f},\ k_\mathrm{t} = 3\hat{\tau} \tag{6}$$

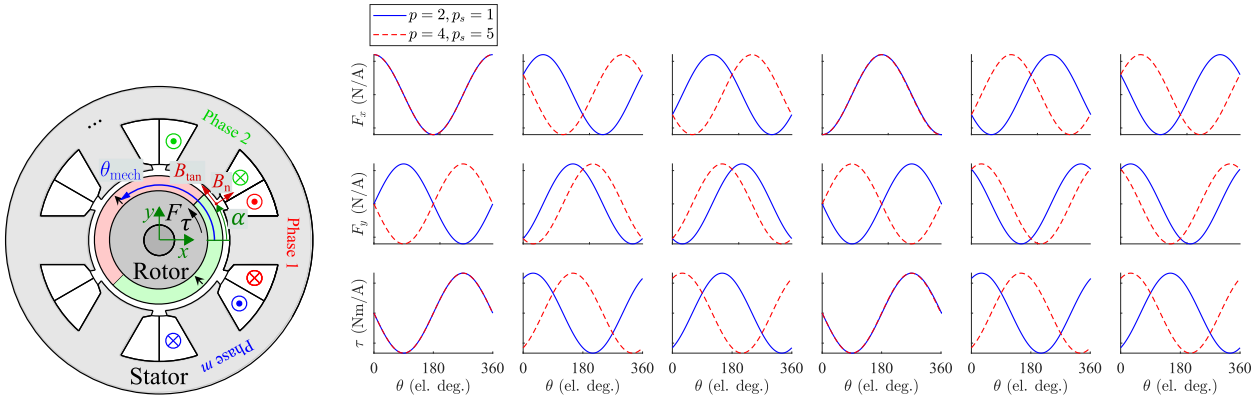

(a) (b)

Fig. 1: (a) PM motor cross-section with the definition of axes and field components, and (b) $\mathbf{T}_{\text{m}}$ matrix for $p = 2$, $p_{\text{s}} = 1$ and $p = 4$, $p_{\text{s}} = 5$ bearingless machines.

2.3. Electric model

The electrical model equations (inductance, back-EMF) are now derived for the winding. The EMF induced in each phase due to the magnetizing field can be calculated using the phase winding function Eq. (1) as:

$$\lambda_k(\theta) = rl\int_0^{2\pi} N_k(\alpha)B_\delta(\alpha)\mathrm{d}\alpha = \underbrace{\pi\hat{N}_p\hat{B}_\delta rl}_{k_{\text{e}}}\cos\left(\theta - [k-1]\alpha_{\text{t}}\right) \quad \Rightarrow \quad e_k = \frac{d\lambda_k}{dt} = k_{\text{e}}\omega\sin\left([k-1]\alpha_{\text{t}} - \theta\right) \tag{7}$$

The inductance of each phase winding can be similarly calculated using winding function theory as

$$L_{j,k} = \mu_0\frac{rl}{\delta}\int_0^{2\pi} N_j(\alpha)N_k(\alpha)\mathrm{d}\alpha = \tfrac{1}{3}\left[L_{\text{t}}\cos\left([k-j]\alpha_{\text{t}}\right) + L_{\text{s}}\cos\left([k-j]\alpha_{\text{s}}\right)\right], \tag{8}$$

where $L_{\text{t}} = 3L_o\hat{N}_p^2$, $L_{\text{s}} = 3L_o\hat{N}_{p_{\text{s}}}^2$, and $L_o = \mu_0\pi\frac{rl}{\delta}$ are common term pairings, e.g. Eq. (29) of Khamitov et al. (2023).

These expressions enable the development of a complete winding electric model of $\mathbf{v}_m = \mathbf{R}\mathbf{i}_m + \mathbf{L}\frac{d}{dt}\mathbf{i}_m + \mathbf{e}_m$, where $\mathbf{e}_m$ is column vector populated by Eq. (7) and the inductance matrix is of the form:

$$\mathbf{L} = \frac{1}{3}\begin{pmatrix} L_{\text{t}} + L_{\text{s}} & L_{\text{t}}\cos\alpha_{\text{t}} + L_{\text{s}}\cos\alpha_{\text{s}} & L_{\text{t}}\cos(2\alpha_{\text{t}}) + L_{\text{s}}\cos(2\alpha_{\text{s}}) & \cdots \\ L_{\text{t}}\cos\alpha_{\text{t}} + L_{\text{s}}\cos\alpha_{\text{s}} & L_{\text{t}} + L_{\text{s}} & L_{\text{t}}\cos\alpha_{\text{t}} + L_{\text{s}}\cos\alpha_{\text{s}} & \cdots \\ L_{\text{t}}\cos(2\alpha_{\text{t}}) + L_{\text{s}}\cos(2\alpha_{\text{s}}) & L_{\text{t}}\cos\alpha_{\text{t}} + L_{\text{s}}\cos\alpha_{\text{s}} & L_{\text{t}} + L_{\text{s}} & \cdots \\ \vdots & \vdots & \vdots & \ddots \end{pmatrix} \tag{9}$$

2.4. Space vector model

It is well known that the Generalized Clarke Transformation (GCT) can be used to transform the voltage and current expressions into space vector equations to yield a compact notation for describing the models developed in Sections 2.2 and 2.3, Khamitov et al. (2023). This transformation is applied to the current expression Eq. (5) to obtain the following space vectors associated with torque and suspension current.

$$\vec{f}_{\text{t}} = f_{\alpha_{\text{t}}} + jf_{\beta_{\text{t}}} = c\sum_{k=1}^{m} f_k e^{j[k-1]\alpha_{\text{t}}}, \;\; \vec{f}_{\text{s}} = f_{\alpha_{\text{s}}} + jf_{\beta_{\text{s}}} = c\sum_{k=1}^{m} f_k e^{j[k-1]\alpha_{\text{s}}} \quad \Rightarrow \quad \vec{i}_{\text{t}} = \hat{I}_{\text{t}}e^{j\theta+\phi'_{\text{t}}}, \;\; \vec{i}_{\text{s}} = \hat{I}_{\text{s}}e^{j\theta+\phi'_{\text{s}}} \;\; \text{for } c = \tfrac{1}{3} \tag{10}$$

The space vectors can be rotated by θ into the synchronous frame as $\vec{i}_{\text{t}}^{\,\text{T}} = \vec{i}_{\text{t}}e^{-j\theta} = \hat{I}_{\text{t}}e^{j\phi'_{\text{t}}}$ and $\vec{i}_{\text{s}}^{\,\text{S}} = \vec{i}_{\text{s}}e^{-j\theta} = \hat{I}_{\text{s}}e^{j\phi'_{\text{s}}}$. Using Eq. (6), these space vectors can be conveniently connected to shaft torque and force as

$$\begin{aligned} &T = T_d + j\tau = k_{\text{t}}\vec{i}_{\text{t}}^{\,\text{T}} = \bar{k}_{\text{t}}\vec{i}_{\text{t}} && \text{where } \bar{k}_{\text{t}} = k_{\text{t}}e^{-j\theta} \text{ and } \vec{i}_{\text{t}}^{\,\text{T}} = i_{\text{d}} + ji_{\text{q}} \\ &\vec{F} = F_{\text{x}} + jF_{\text{y}}, \quad \left.\begin{matrix} p_{\text{s}} = p+1: \;\; F_{\text{x}} + jF_{\text{y}} \\ p_{\text{s}} = p-1: \;\; F_{\text{x}} - jF_{\text{y}} \end{matrix}\right\} = k_{\text{f}}\vec{i}_{\text{s}}^{\,\text{S}} = \bar{k}_{\text{f}}\vec{i}_{\text{s}} && \text{where } \bar{k}_{\text{f}} = k_{\text{f}}e^{-j\theta} \text{ and } \vec{i}_{\text{s}}^{\,\text{S}} = i_{\text{x}} + ji_{\text{y}} \end{aligned} \tag{11}$$

The GCT can be similarly applied to the electric model of Section 2.3 to arrive at

$$\vec{v}_{\text{t}} = L_{\text{t}}\tfrac{\mathrm{d}}{\mathrm{d}t}\vec{i}_{\text{t}} + R\vec{i}_{\text{t}} + \vec{e}_{\text{m}}, \qquad \vec{v}_{\text{s}} = L_{\text{s}}\tfrac{\mathrm{d}}{\mathrm{d}t}\vec{i}_{\text{s}} + R\vec{i}_{\text{s}} \tag{12}$$

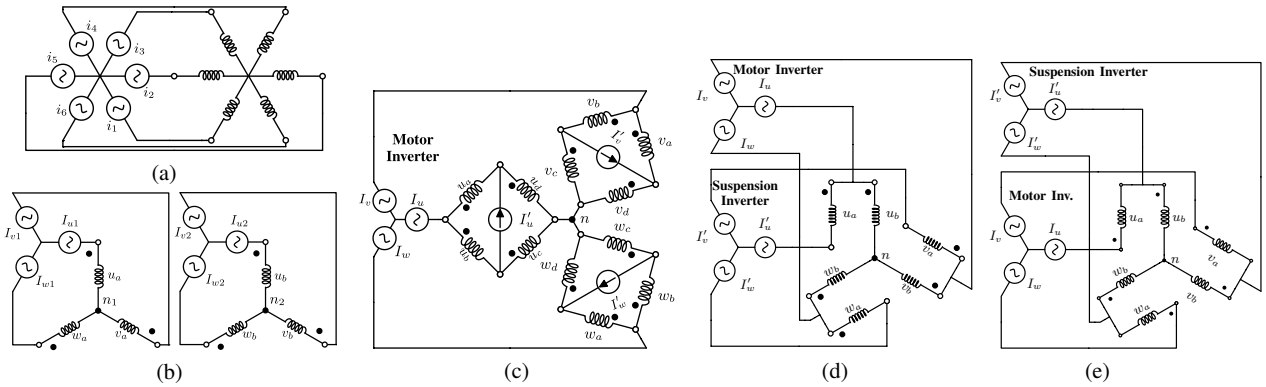

Fig. 2: Combined windings: (a) multiphase winding with single neutral point (MP), (b) multiphase winding with dual neutral point (MP2), (c) bridge, (d) parallel, and (e) MCI.

3. Proposed universal model

In addition to multiphase combined windings, research literature has independently developed three other types of combined windings: bridge (Khoo et al. (2002)), mid-point current injection (Chiba et al. (2011)), and parallel windings (Oishi et al. (2013)), shown in Fig. 2. It was shown in Khamitov and Severson (2023) that these winding types are actually multiphase windings where the phases are connected to the drive electronics in unique configurations to achieve distinct objectives (i.e., eliminate back-EMF at the suspension inverter). This means that the force / torque and electric models for these windings can be derived from the multiphase winding. Such derivations are provided in Table I of Khamitov et al. (2023) and Section V of Petersen and Severson (2025).

This section summarizes the equivalencies of combined windings, presents transformation matrices between winding types, and proposes the paper's universal model that is applicable to all combined winding bearingless motors.

3.1. Transformation to combined winding using space vector model

To create the torque and force indicated in Eq. (6), the parallel, bridge, and MCI drives must 1) control currents in the MP phases, as described in Eq. (5), and 2) connect the MP winding phases to the drive electronics in the manner shown in Fig. 2. To accomplish this, a deliberate assignment must be made of the MP phases (phase 1, 2, ... 6) to the coil group labels of "u_a", "u_b", etc. of Fig. 2 as described in Table I of Khamitov et al. (2023) and summarized later in Table 4.

The windings must control the terminal currents listed in Table 1, where $\vec{i}_{\mathrm{t}}$ and $\vec{i}_{\mathrm{s}}$ are the space vectors calculated in Eq. (10). The superscript * indicates a complex conjugate and the subscript $_{\mathrm{term}}$ indicates the terminal current space vectors, which correspond to the currents entering the three phase "motor" and "suspension" terminals in Fig. 2 using the standard three phase Clarke Transform. Notice that the space vector model to control these windings has been developed in the literature in a similar form to Eq. (11) and (12), but described from the perspective of each winding's terminal currents and voltages. In this case, the suspension current vector $\vec{i}_{\mathrm{s},w}$ rotates in the opposite direction to the torque current vector $\vec{i}_{\mathrm{t},w}$, as indicated by the complex conjugate in the "Control Currents" row (see Table 1). This difference in rotation direction must be carefully considered to calculate shaft torque and force in Eq. (13), where two different force vector are defined depending on whether $p_{\mathrm{s}} = p+1$ or $p_{\mathrm{s}} = p-1$. In Eq. (13), $\bar{k}_{\mathrm{t},w}$, $\bar{k}_{\mathrm{f},w}$, $\vec{i}_{\mathrm{t},w}$, and $\vec{i}_{\mathrm{s},w}$ are the machine parameters found in the literature for these windings, while $\vec{i}_{\mathrm{t}}^{\mathrm{T}}$, $\vec{i}_{\mathrm{s}}^{\mathrm{S}}$ remain the synchronous frame space vectors used in Eq. (11). Notice that the y-direction force is reversed as compared to Eq. (11); this is a consequence of $\vec{i}_{\mathrm{s},w}$ rotating in the $-\theta$ direction.

$$
\begin{aligned}
&T = T_d + j\tau = k_{\mathrm{t}}\vec{i}_{\mathrm{t}}^{\mathrm{T}} = \bar{k}_{\mathrm{t},w}\vec{i}_{\mathrm{t},w} && \text{using } \bar{k}_{\mathrm{t},w} \text{ and } \vec{i}_{\mathrm{t},w} \text{ from Table 1} \\
&\vec{F} = F_{\mathrm{x}} + jF_{\mathrm{y}}, \quad \left.\begin{array}{ll} p_{\mathrm{s}} = p+1: & F_{\mathrm{x}} - jF_{\mathrm{y}} \\ p_{\mathrm{s}} = p-1: & F_{\mathrm{x}} + jF_{\mathrm{y}} \end{array}\right\} = k_{\mathrm{f}}\vec{i}_{\mathrm{s}}^{\mathrm{s}*} = \bar{k}_{\mathrm{f},w}\vec{i}_{\mathrm{s},w} && \text{using } \bar{k}_{\mathrm{f},w} \text{ and } \vec{i}_{\mathrm{s},w} \text{ from Table 1}
\end{aligned} \tag{13}
$$

Terminal and control voltage vectors in Tables 1 and 2 relate electric models reported in literature to the MP electric model. These differential equations are used to design current regulators to control force and torque. Effective controller design (particularly of feedforward decoupling terms) has been the subject of several papers, e.g. Petersen et al. (2021).

Table 1: Space vector model of the circuit-based combined windings in terms of the MP winding quantities

	Bridge	**Parallel**	**MCI**	**MP2**
Terminal Currents	$\vec{i}_{\mathrm{t,term}} = 2\vec{i}_{\mathrm{t}} \quad \vec{i}_{\mathrm{s,term}} = 2\vec{i}_{\mathrm{s}}^{*}$	$\vec{i}_{\mathrm{t,term}} = 2\vec{i}_{\mathrm{t}} \quad \vec{i}_{\mathrm{s,term}} = -\vec{i}_{\mathrm{t}} + \vec{i}_{\mathrm{s}}^{*}$	$\vec{i}_{\mathrm{t,term}} = \vec{i}_{\mathrm{t}} - \vec{i}_{\mathrm{s}}^{*} \quad \vec{i}_{\mathrm{s,term}} = 2\vec{i}_{\mathrm{s}}^{*}$	$\vec{i}_{1,\mathrm{term}} = \vec{i}_{\mathrm{t}} - \vec{i}_{\mathrm{s}}^{*} \quad \vec{i}_{2,\mathrm{term}} = \vec{i}_{\mathrm{t}} + \vec{i}_{\mathrm{s}}^{*}$
Control Currents $\vec{i}_{\mathrm{t},w}$, $\vec{i}_{\mathrm{s},w}$	$\vec{i}_{\mathrm{t,B}} = 2\vec{i}_{\mathrm{t}} \quad \vec{i}_{\mathrm{s,B}} = 2\vec{i}_{\mathrm{s}}^{*}$	$\vec{i}_{\mathrm{t,P}} = 2\vec{i}_{\mathrm{t}} \quad \vec{i}_{\mathrm{s,P}} = \vec{i}_{\mathrm{s}}^{*}$	$\vec{i}_{\mathrm{t,MCI}} = \vec{i}_{\mathrm{t}} \quad \vec{i}_{\mathrm{s,MCI}} = 2\vec{i}_{\mathrm{s}}^{*}$	$\vec{i}_{\mathrm{t,MP2}} = \vec{i}_{\mathrm{t}} \quad \vec{i}_{\mathrm{s,MP2}} = \vec{i}_{\mathrm{s}}^{*}$
Torque $\bar{k}_{\mathrm{t},w}$	$\bar{k}_{\mathrm{t,B}} = \frac{k_{\mathrm{t}}}{2} e^{-j\theta}$	$\bar{k}_{\mathrm{t,P}} = \frac{k_{\mathrm{t}}}{2} e^{-j\theta}$	$\bar{k}_{\mathrm{t,MCI}} = k_{\mathrm{t}} e^{-j\theta}$	$\bar{k}_{\mathrm{t,MP2}} = k_{\mathrm{t}} e^{-j\theta}$
Force $\bar{k}_{\mathrm{f},w}$	$\bar{k}_{\mathrm{f,B}} = \frac{k_{\mathrm{f}}}{2} e^{j\theta}$	$\bar{k}_{\mathrm{f,P}} = k_{\mathrm{f}} e^{j\theta}$	$\bar{k}_{\mathrm{f,MCI}} = \frac{k_{\mathrm{f}}}{2} e^{j\theta}$	$\bar{k}_{\mathrm{f,MP2}} = k_{\mathrm{f}} e^{j\theta}$

Table 2: Terminal and control voltage equations

	Torque	**Suspension**
Bridge	$\vec{v}_{\mathrm{t,term}} = \vec{v}_{\mathrm{t,B}} = \frac{L_{\mathrm{t}}}{2}\frac{\mathrm{d}}{\mathrm{d}t}\vec{i}_{\mathrm{t,B}} + \frac{R}{2}\vec{i}_{\mathrm{t,B}} + \vec{e}_{\mathrm{m}}$	$\vec{v}_{\mathrm{s,term}} = \vec{v}_{\mathrm{s,B}} = \frac{L_{\mathrm{s}}}{2}\frac{\mathrm{d}}{\mathrm{d}t}\vec{i}_{\mathrm{s,B}} + \frac{R}{2}\vec{i}_{\mathrm{s,B}}$
Parallel	$\vec{v}_{\mathrm{t,term}} = \overbrace{\frac{L_{\mathrm{t}}}{2}\frac{\mathrm{d}}{\mathrm{d}t}\vec{i}_{\mathrm{t,P}} + \frac{R}{2}\vec{i}_{\mathrm{t,P}} + \vec{e}_{\mathrm{m}}}^{\vec{v}_{\mathrm{t,P}}} + \overbrace{R\vec{i}_{\mathrm{s,P}} + L_{\mathrm{s}}\frac{\mathrm{d}}{\mathrm{d}t}\vec{i}_{\mathrm{s,P}}}^{\text{cross-coupling}}$	$\vec{v}_{\mathrm{s,term}} = \vec{v}_{\mathrm{s,P}} = 2L_{\mathrm{s}}\frac{\mathrm{d}}{\mathrm{d}t}\vec{i}_{\mathrm{s,P}} + 2R\vec{i}_{\mathrm{s,P}}$
MCI	$\vec{v}_{\mathrm{t,term}} = \vec{v}_{\mathrm{t,MCI}} = 2L_{\mathrm{t}}\frac{\mathrm{d}}{\mathrm{d}t}\vec{i}_{\mathrm{t,MCI}} + 2R\vec{i}_{\mathrm{t,MCI}} + 2\vec{e}_{\mathrm{m}}$	$\vec{v}_{\mathrm{s,term}} = \overbrace{\frac{L_{\mathrm{s}}}{2}\frac{\mathrm{d}}{\mathrm{d}t}\vec{i}_{\mathrm{s,MCI}} + \frac{R}{2}\vec{i}_{\mathrm{s,MCI}} + \vec{e}_{\mathrm{m}}}^{\vec{v}_{\mathrm{s,MCI}}} + \overbrace{R\vec{i}_{\mathrm{t,MCI}} + L_{\mathrm{t}}\frac{\mathrm{d}}{\mathrm{d}t}\vec{i}_{\mathrm{t,MCI}}}^{\text{cross-coupling}}$
MP2	$\vec{v}_{1,\mathrm{term}} = \overbrace{L_{\mathrm{t}}\frac{\mathrm{d}}{\mathrm{d}t}\vec{i}_{\mathrm{t,MP2}} + R\vec{i}_{\mathrm{t,MP2}} + \vec{e}_{\mathrm{m}}}^{\vec{v}_{\mathrm{t,MP2}}=\vec{v}_{\mathrm{t}}} - \overbrace{R\vec{i}_{\mathrm{s,MP2}} - L_{\mathrm{s}}\frac{\mathrm{d}}{\mathrm{d}t}\vec{i}_{\mathrm{s,MP2}}}^{\text{cross-coupling}}$	$\vec{v}_{2,\mathrm{term}} = \overbrace{L_{\mathrm{s}}\frac{\mathrm{d}}{\mathrm{d}t}\vec{i}_{\mathrm{s,MP2}} + R\vec{i}_{\mathrm{s,MP2}} + \vec{e}_{\mathrm{m}}}^{\vec{v}_{\mathrm{s,MP2}}} + \overbrace{R\vec{i}_{\mathrm{t,MP2}} + L_{\mathrm{t}}\frac{\mathrm{d}}{\mathrm{d}t}\vec{i}_{\mathrm{t,MP2}}}^{\text{cross-coupling}}$

3.2. Proposed universal bearingless motor model

This paper proposes the generalized bearingless motor model shown in Fig. 3. This model is developed with the perspective of Section 2 (MP winding) containing the fundamental information of the machine. When the winding is connected to drive electronics in a different configuration (i.e., bridge, parallel, MCI, and MP2), the terminal voltages and currents are transformed into the phase voltages and currents of the MP winding model, the MP governing equations for shaft force/torque (Section 2.2) and voltage/current (Section 2.3) are used to model the machine's behavior, and then the resulting currents are transformed back to the resulting terminal currents.

The proposed model (Fig. 3) is now described in detail. The model input $\mathbf{v}_{\mathrm{term}}$ is the voltage applied at the terminals of the motor relative to its neutral. For Fig. 2a, $\mathbf{v}_{\mathrm{term}} = \mathbf{v}_m$ and for Fig. 2b-d, $\mathbf{v}_{\mathrm{term}} = [v_u, v_v, v_w, v'_u, v'_v, v'_w]^T$. This is converted to the coil group voltage $\mathbf{v}_{m'} = [v_{ua}, v_{ub}, v_{va}, v_{vb}, v_{wa}, v_{wb}]^T$ using the transformation matrix $T^{\mathrm{v,term}}_{\mathrm{v},m'}$ presented in Table 3. Note that in this paper's nomenclature, $T^{\mathrm{v,term}}_{\mathrm{v},m'} = \left(T^{\mathrm{v},m'}_{\mathrm{v,term}}\right)^{-1}$ and $T^{\mathrm{v},m'}_{\mathrm{v,term}}$ is equivalent to the matrix $T^{\mathrm{v},m}_{\mathrm{v,ph}}$ introduced in Section V of Petersen and Severson (2025). Next, $\mathbf{v}_{m'}$ is converted to the voltage across each phase of the MP winding $\mathbf{v}_m$ through the matrix $T^{m'}_{m}$ of Table 4. This matrix depends on the number of pole-pairs p, p_{s} through Eq. (2) and implements the mapping summarized in Table I of Khamitov et al. (2023); Petersen and Severson (2025).

The MP phase voltage $\mathbf{v}_m$ is applied to the winding electric model (Section 2.3) to determine the MP phase current $\mathbf{i}_m$. The $\mathbf{T}_{\mathrm{m}}$ matrix of Section 2.2 is multiplied by the phase currents to determine the shaft force and torque.

The MP phase currents $\mathbf{i}_m$ are converted to coil group currents $\mathbf{i}_{m'} = [i_{ua}, i_{ub}, i_{va}, i_{vb}, i_{wa}, i_{wb}]$ by $T^{\mathrm{i},m'}_{\mathrm{i,term}}$ provided in Table 3. Here, positive currents enter the dotted terminals of Fig. 2. The coil group currents are then converted to terminal currents $\mathbf{i}_{\mathrm{term}}$ using $T^{\mathrm{i},m'}_{\mathrm{i,term}}$, where for Fig. 2a, $\mathbf{i}_{\mathrm{term}} = \mathbf{i}_m$ and for Fig. 2b-d, $\mathbf{i}_{\mathrm{term}} = [I_u, I_v, I_w, I'_u, I'_v, I'_w]^T$, with current defined as positive entering the motor. The paper considers that coil groups c and d of the bridge winding are created by splitting the coil groups a and b in half. From this, the inverse of $T^{\mathrm{v},m'}_{\mathrm{v,term}}$ and $T^{\mathrm{i},m'}_{\mathrm{i,term}}$ are calculated by assuming that the voltage of coil groups a and c, and coil groups b and d are equal in each phase (e.g. $v_{ua} = v_{uc}$ and $v_{ub} = v_{ud}$), and that the torque and suspension terminal currents split equally between the two parallel paths.

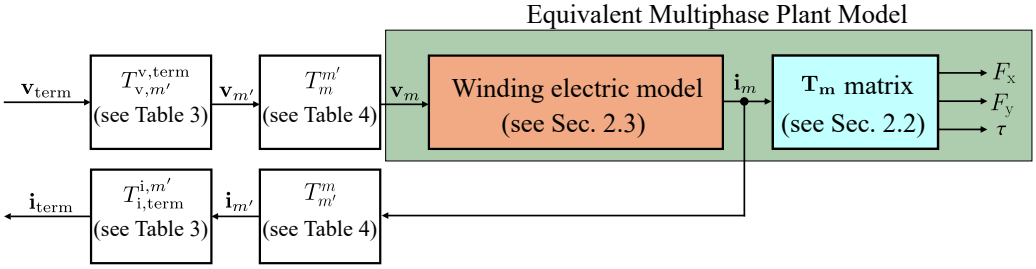

Fig. 3: Proposed universal bearingless motor model

Table 3: Voltage and current coil-group to terminal transformation matrices

	Bridge	Parallel	MCI	MP2
$T^{\mathrm{v},m'}_{\mathrm{v,term}}$	$\begin{bmatrix} 1 & 0 & 0 & 1 & 0 & 0 & 0 & 0 & 0 & 0 & 0 & 0 \\ 0 & 0 & 0 & 0 & 1 & 0 & 0 & 1 & 0 & 0 & 0 & 0 \\ 0 & 0 & 0 & 0 & 0 & 0 & 0 & 0 & 1 & 0 & 0 & 1 \\ 0 & 0 & -1 & 1 & 0 & 0 & 0 & 0 & 0 & 0 & 0 & 0 \\ 0 & 0 & 0 & 0 & 0 & 0 & -1 & 1 & 0 & 0 & 0 & 0 \\ 0 & 0 & 0 & 0 & 0 & 0 & 0 & 0 & 0 & 0 & -1 & 1 \end{bmatrix}$	$\begin{bmatrix} 0 & 1 & 0 & 0 & 0 & 0 \\ 0 & 0 & 0 & 1 & 0 & 0 \\ 0 & 0 & 0 & 0 & 0 & 1 \\ -1 & 1 & 0 & 0 & 0 & 0 \\ 0 & 0 & -1 & 1 & 0 & 0 \\ 0 & 0 & 0 & 0 & -1 & 1 \end{bmatrix}$	$\begin{bmatrix} 1 & 1 & 0 & 0 & 0 & 0 \\ 0 & 0 & 1 & 1 & 0 & 0 \\ 0 & 0 & 0 & 0 & 1 & 1 \\ 0 & 1 & 0 & 0 & 0 & 0 \\ 0 & 0 & 0 & 1 & 0 & 0 \\ 0 & 0 & 0 & 0 & 0 & 1 \end{bmatrix}$	$\begin{bmatrix} 1 & 0 & 0 & 0 & 0 & 0 \\ 0 & 0 & 1 & 0 & 0 & 0 \\ 0 & 0 & 0 & 0 & 1 & 0 \\ 0 & 1 & 0 & 0 & 0 & 0 \\ 0 & 0 & 0 & 1 & 0 & 0 \\ 0 & 0 & 0 & 0 & 0 & 1 \end{bmatrix}$
$T^{\mathrm{i},m'}_{\mathrm{i,term}}$	$\begin{bmatrix} 1 & 1 & 0 & 0 & 0 & 0 & 0 & 0 & 0 & 0 & 0 & 0 \\ 0 & 0 & 0 & 0 & 1 & 1 & 0 & 0 & 0 & 0 & 0 & 0 \\ 0 & 0 & 0 & 0 & 0 & 0 & 0 & 0 & 1 & 1 & 0 & 0 \\ -1 & 0 & 0 & 1 & 0 & 0 & 0 & 0 & 0 & 0 & 0 & 0 \\ 0 & 0 & 0 & 0 & -1 & 0 & 0 & 1 & 0 & 0 & 0 & 0 \\ 0 & 0 & 0 & 0 & 0 & 0 & 0 & -1 & 0 & 0 & 1 & 1 \end{bmatrix}$	$\begin{bmatrix} 1 & 1 & 0 & 0 & 0 & 0 \\ 0 & 0 & 1 & 1 & 0 & 0 \\ 0 & 0 & 0 & 0 & 1 & 1 \\ -1 & 0 & 0 & 0 & 0 & 0 \\ 0 & 0 & -1 & 0 & 0 & 0 \\ 0 & 0 & 0 & -1 & 0 & 0 \end{bmatrix}$	$\begin{bmatrix} 1 & 0 & 0 & 0 & 0 & 0 \\ 0 & 0 & 1 & 0 & 0 & 0 \\ 0 & 0 & 0 & 0 & 1 & 0 \\ -1 & 1 & 0 & 0 & 0 & 0 \\ 0 & 0 & -1 & 1 & 0 & 0 \\ 0 & 0 & 0 & 0 & -1 & 1 \end{bmatrix}$	$\begin{bmatrix} 1 & 0 & 0 & 0 & 0 & 0 \\ 0 & 0 & 1 & 0 & 0 & 0 \\ 0 & 0 & 0 & 0 & 1 & 0 \\ 0 & 1 & 0 & 0 & 0 & 0 \\ 0 & 0 & 0 & 1 & 0 & 0 \\ 0 & 0 & 0 & 0 & 0 & 1 \end{bmatrix}$

Table 4: Mapping matrices from 6-phase MP to Parallel DPNV, MCI, and MP2 coil groups ($T^{m}_{m'}$)

	Case 1 $\alpha_{\mathrm{t}} = +\pi/3$ $\alpha_{\mathrm{s}} = +2\pi/3$	Case 2 $\alpha_{\mathrm{t}} = +2\pi/3$ $\alpha_{\mathrm{s}} = +\pi/3$	Case 3 $\alpha_{\mathrm{t}} = -\pi/3$ $\alpha_{\mathrm{s}} = -2\pi/3$	Case 4 $\alpha_{\mathrm{t}} = -2\pi/3$ $\alpha_{\mathrm{s}} = -\pi/3$
$[u_a, u_b, v_a, v_b, w_a, w_b]$	$[-4, +1, -6, +3, -2, +5]$	$[+4, +1, +2, +5, +6, +3]$	$[-4, +1, -2, +5, -6, +3]$	$[+4, +1, +6, +3, +2, +5]$
$T^{m}_{m'}$	$\begin{bmatrix} 0 & 0 & 0 & -1 & 0 & 0 \\ 1 & 0 & 0 & 0 & 0 & 0 \\ 0 & 0 & 0 & 0 & 0 & -1 \\ 0 & 0 & 1 & 0 & 0 & 0 \\ 0 & -1 & 0 & 0 & 0 & 0 \\ 0 & 0 & 0 & 0 & 1 & 0 \end{bmatrix}$	$\begin{bmatrix} 0 & 0 & 0 & 1 & 0 & 0 \\ 1 & 0 & 0 & 0 & 0 & 0 \\ 0 & 1 & 0 & 0 & 0 & 0 \\ 0 & 0 & 0 & 0 & 1 & 0 \\ 0 & 0 & 0 & 0 & 0 & 1 \\ 0 & 0 & 1 & 0 & 0 & 0 \end{bmatrix}$	$\begin{bmatrix} 0 & 0 & 0 & -1 & 0 & 0 \\ 1 & 0 & 0 & 0 & 0 & 0 \\ 0 & -1 & 0 & 0 & 0 & 0 \\ 0 & 0 & 0 & 0 & 1 & 0 \\ 0 & 0 & 0 & 0 & 0 & -1 \\ 0 & 0 & 1 & 0 & 0 & 0 \end{bmatrix}$	$\begin{bmatrix} 0 & 0 & 0 & 1 & 0 & 0 \\ 1 & 0 & 0 & 0 & 0 & 0 \\ 0 & 0 & 0 & 0 & 0 & 1 \\ 0 & 0 & 1 & 0 & 0 & 0 \\ 0 & 1 & 0 & 0 & 0 & 0 \\ 0 & 0 & 0 & 0 & 1 & 0 \end{bmatrix}$

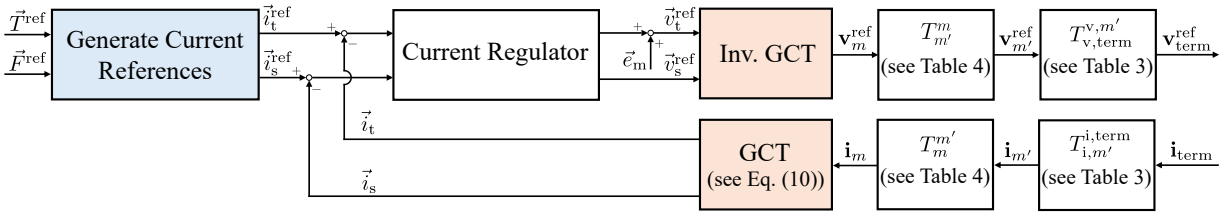

Fig. 4: Proposed universal force and torque controller; see Fig. 5 for details of the "Generate Current References" block.

4. Universal force and torque controller

This section introduces a torque/force controller applicable to bearingless motors with any winding configuration and combination of p and p_s, shown in Fig. 4. The controller is implemented using an analogous approach to the model of Section 3.2: the controller acts on the MP electric model (Section 2.4) by transforming terminal currents/voltages of each specific winding to MP currents/voltages.

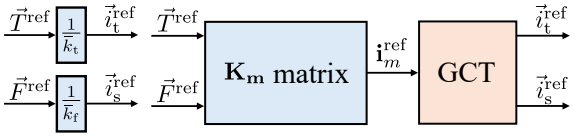

Fig. 5: Generation of current references based on force/torque commands: (a) space vector approach, (b) $\mathbf{K}_{\mathrm{m}}$ matrix approach.

In Fig. 4, the "Generate Current References" block converts torque $\vec{T}^{\mathrm{ref}}$ and force $\vec{F}^{\mathrm{ref}}$ commands into current references. Figure 5 illustrates two implementations: 1) a space vector calculation (Fig. 5a) obtained by solving Eq. (11) and 2) a more general matrix based approach (Fig. 5b), Silber and Amrhein (2000); Khamitov et al. (2021). The matrix approach does not require sinusoidal entries in the $\mathbf{T}_{\mathrm{m}}$ matrix and is suited for bearingless motor systems with higher-order force and torque harmonics. Note in Fig. 5a, $\vec{F}^{\mathrm{ref}}$ should be replaced by $\vec{F}^{\mathrm{ref}*}$ for $p_{\mathrm{s}} = p - 1$ machines, see Eq. (11).

In the "Current Regulator" block, well-known control strategies can be used, such as vector PI control or complex vector current regulation, implemented either in the stationary or synchronous frame, as discussed in Petersen et al. (2021). Regardless of the specific current regulator or winding configurations, the proposed controller always see the plant of the MP winding in Eq. (12). This allows the current regulator to be tuned using only L_{t}, L_{s}, and R. The cross-coupling voltages between torque and suspension terminals observed in Parallel, MCI, and MP2 windings (see Table 2) are handled automatically via the transformation matrices of Tables 3 and 4 as a feedforward compensation.

In summary, the proposed generalized controller allows a bearingless motor with any combined winding type to be designed for the plant model of the multiphase winding configuration. This illustrates the equivalence of these machines and provides a starting point for winding-specific controller development.

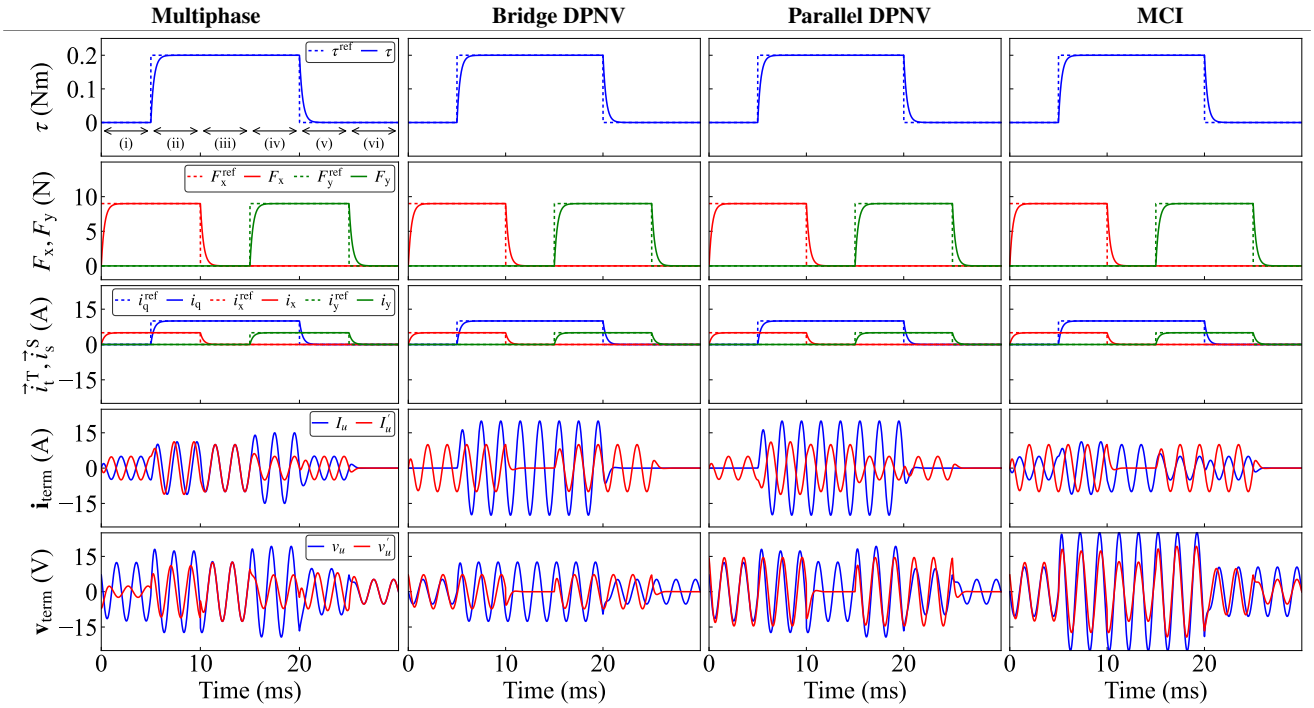

Fig. 6: Simulink simulation results using the proposed universal controller and model.

5. Simulink model

Table 5: Model parameters

Parameter	Value
L_t	0.3 mH
L_s	0.45 mH
R	0.3 Ω
k_e	6.67 mV/(rad/s)
k_t	0.02 Nm/A
k_f	1.8 N/A

This section presents the implementation of the generalized bearingless motor model (Fig. 3) and controller (Fig. 4) in Simulink. The resulting model files are published publicly in the authors' GitHub repository, available at `https://github.com/severson-group/bm-modeling`. Readers can download and run the main script to reproduce the results shown in this section.

The Simulink model enables simulations based on user-specified winding configurations and motor parameters. A MATLAB setup script is provided where users indicate the winding type and the parameters of Eq. (11) and (12). The Simulink files automatically apply the corresponding transformations and controller tuning. The current regulators are implemented as synchronous frame PI controllers. The files are developed in a modular fashion, so that users can replace components and adapt it to meet the specifics of their machine and control environment. For example, replacing the generalized controller with a controller specific to their winding type, or replacing the generalized model with a motor/winding-specific model.

Example simulation results for an $p = 4$ and $p_s = 5$ bearingless machine configured with MP, bridge DPNV, parallel DPNV, and MCI windings are presented in Fig. 6. The machine has the model parameters summarized in Table 5. In this simulation, step force and torque commands are issued (first two rows) while the shaft is spinning at 7800 RPM.

The third row shows the torque and suspension currents of Eq. (11) in the synchronous frame. As expected, these currents are identical across all winding configurations, demonstrating that the proposed generalized model treats all currents as the equivalent multiphase winding model. In contrast, the forth row shows the terminal currents in phase U, which differ for each winding configuration. For example, during region (i), where only F_x^{ref} is issued, the bridge and parallel windings contain only suspension currents, whereas the multiphase and MCI windings contain both torque and suspension currents. This is especially evident in the MCI configuration, where half of the suspension current appears on the torque terminals. Similarly, in region (iii), where only τ^{ref} is generated, half of the torque current appears on the suspension terminals in the parallel DPNV winding.

The fifth row shows the terminal voltage in phase U. Again, notable differences can be observed for each winding type. This is best illustrated during region (vi), where although all force and torque currents are zero, back-EMF is induced at the torque terminals of all windings; however, for the bridge DPNV and parallel DPNV winding, no back-EMF appears on the suspension terminals, clearly demonstrating the DPNV property of these windings.

In summary, the proposed universal model/controller enables all combined windings to be treated within the equiv-

alent multiphase winding model through transformation matrices and to use a single set of controller tuning parameters. This is verified through Simulink simulations and shown to yield equivalent step force and torque results for all windings.

6. Conclusion

This paper presents a generalized simulation model for bearingless motors that accommodates all types of combined winding configurations, aiming to support ongoing and future research in this domain. The model and controller are developed based on calculating the phase voltage and current of the winding, when it is viewed as a multiphase winding, from the terminal voltages and currents of any combined winding configuration. The paper finds that this allows for the creation of 1) a universal model of the force/torque and voltage/current behavior of the machine and 2) a universal control implementation where the same current regulator can be applied to any combined winding bearingless motor without needing to re-tune the controller gains when switching between winding types.

Note that the universal controller is unlikely to be used as the final control implementation of a bearingless motor. This is especially true in bridge, parallel, and MCI combined windings, where the goal of using these windings is typically to enable the use of separate motor and suspension inverters and controllers and therefore a single combined motor/force controller is not viable. Instead, the proposed universal controller/model provide a trusted starting point for control development and simulation. As a user's control architecture matures, they are expected to progressively replace "universal" components with architecture-specific components. For example, in a bridge winding, first changing the universal controller to separate torque and force controllers, then replacing the model with a true 12 coil-group machine, and then introducing single and three phase inverters, and so on until the simulation environment fully reflects their hardware. At each step, users can compare simulation results with the trusted universal controller/model to ensure proper functionality.

References

Chiba, A., Sotome, K., Iiyama, Y., and Rahman, M. A. (2011). A novel middle-point-current-injection-type bearingless pm synchronous motor for vibration suppression. *IEEE Transactions on Industry Applications*, 47(4):1700–1706.

Gruber, W. and Silber, S. (2018). Dual field-oriented control of bearingless motors with combined winding system. In *2018 International Power Electronics Conference (IPEC-Niigata 2018-ECCE Asia)*, pages 4028–4033. IEEE.

Khamitov, A., Gruber, W., Bramerdorfer, G., and Severson, E. L. (2021). Comparison of combined winding strategies for radial nonsalient bearingless machines. *IEEE Transactions on Industry Applications*, 57(6):6856–6869.

Khamitov, A., Petersen, N. P., and Severson, E. L. (2023). Combined windings for bearingless motors—an overview. In *2023 IEEE Energy Conversion Congress and Exposition (ECCE)*, pages 4628–4635. IEEE.

Khamitov, A. and Severson, E. L. (2023). Design of multi-phase combined windings for bearingless machines. *IEEE Transactions on Industry Applications*, 59(3):3243–3255.

Khoo, W., Fittro, R. L., and Garvey, S. D. (2002). Ac polyphase self-bearing motors with a bridge configured winding. In *Proc. 7th International Symposium on Magnetic Bearings*, pages 47–52.

Oishi, R., Horima, S., Sugimoto, H., and Chiba, A. (2013). A novel parallel motor winding structure for bearingless motors. *IEEE Transactions on Magnetics*, 49(5):2287–2290.

Petersen, N., Khamitov, A., Slininger, T., and Severson, E. L. (2021). Machine design and precision current regulation for the parallel dpnv bearingless motor winding. *IEEE Transactions on Industry Applications*, 57(6):7000–7011.

Petersen, N. P. and Severson, E. L. (2025). Rotor eccentricity impact on electromagnetic behavior in combined winding bearingless motors towards displacement self-sensing. *IEEE Transactions on Energy Conversion*, 40(1):323–336.

Silber, S. and Amrhein, W. (2000). Power optimal current control scheme for bearingless pm motors. In *Proc. 7th International Symposium on Magnetic Bearings*, pages 401–406.

Silber, S., Amrhein, W., Bosch, P., Schob, R., and Barletta, N. (2005). Design aspects of bearingless slice motors. *IEEE/ASME Transactions on Mechatronics*, 10(6):611–617.

Sung, D., Noguchi, T., Kang, S.-G., and Severson, E. (2025). System identification and sensor calibration methods for commissioning of bearingless machines. In *19th International Symposium on Magnetic Bearings*, pages 1–8. ISMB.